First-Principles Prediction of Spin-Polarized Multiple Dirac Rings in Manganese Fluoride

Yalong Jiao,[1] Fengxian Ma,[1] Chunmei Zhang,[1] John Bell,[1] Stefano Sanvito,[2] and Aijun Du[1,*]
[1]School of Chemistry, Physics and Mechanical Engineering, Queensland University of Technology, Gardens Point Campus, Brisbane, Queensland 4001, Australia
[2]School of Physics, AMBER and CRANN Institute, Trinity College, Dublin 2, Ireland
(Received 7 February 2017; revised manuscript received 14 May 2017; published 7 July 2017)

Spin-polarized materials with Dirac features have sparked great scientific interest due to their potential applications in spintronics. But such a type of structure is very rare and none has been fabricated. Here, we investigate the already experimentally synthesized manganese fluoride (MnF_3) as a novel spin-polarized Dirac material by using first-principles calculations. MnF_3 exhibits multiple Dirac cones in one spin orientation, while it behaves like a large gap semiconductor in the other spin channel. The estimated Fermi velocity for each cone is of the same order of magnitude as that in graphene. The 3D band structure further reveals that MnF_3 possesses rings of Dirac nodes in the Brillouin zone. Such a spin-polarized multiple Dirac ring feature is reported for the first time in an experimentally realized material. Moreover, similar band dispersions can be also found in other transition metal fluorides (e.g., CoF_3, CrF_3, and FeF_3). Our results highlight a new interesting single-spin Dirac material with promising applications in spintronics and information technologies.

DOI: 10.1103/PhysRevLett.119.016403

Ever since the spin and charge of one electron have been considered separately, it has been found that the spin current displays superior properties to the classical charge current in the field of information transmission such as high speed, low power consumption, and negligible energy dissipation [1]. Thus, the corresponding spin current has drawn great attention over the past few decades and the spin electronics are rapidly expanding [2–11]. Up to now, a number of spintronics materials have been proposed including magnetic metals, half-metallic ferromagnets, topological insulators, magnetic semiconductors, diluted magnetic semiconductors, etc. [12–16]. But to exploit the full potential of spintronics in information transfer and storage, some basic issues still remain, such as long distance spin transport, and the generation and injection of spin polarized currents [4,17,18]. In addition to them, the grand challenges for new generation spintronics are how to make electrons transport with ultrahigh speed and consume ultralow energy, which requires realizing massless electrons by discovering the potential Dirac band dispersion, and achieve dissipationless spin transport via generating large spin polarization around the Fermi level [19].

It is necessary to emphasize that the well-studied materials for spintronics such as half-metals, can meet the "basic" demand of spintronics applications [20,21]. In addition, Wang [22] proposed a new class of materials named spin gapless semiconductors (SGS) that can generate 100% spin polarized current and is promising in spintronics. The SGS was then validated by Ouardi *et al.* in experiment [23]. However, to overcome the "grand challenge," the performances of half-metal and SGS are still limited as it just behaves like a metal-semiconductor in one spin orientation, but lacks linear Dirac dispersion, which can hardly reach the goal of ultrahigh speed spin transport. Therefore, it is of great interest to explore new platforms with spin-polarized linear energy dispersion (Dirac half-metal) and massless Dirac fermions, which will lead towards realistic applications in high effieciency spintronics and quantum information technologies [19,24,25]. Dirac materials with spin-polarized band structures can effectively utilize spin degrees of freedom of electrons. They can also break the protection of time-reversal symmetry (TRS) but maintain the linear relation of energy-momentum dispersion at the Fermi level, resulting in outstanding transport properties. Such a type of material was theoretically proposed in a triangular ferrimagnet in recent years [24], but this novel class of structures is very rare and has only been predicted in a limited number of configurations such as CrO_2/TiO_2 heterostructure [26], Mn-intercalated graphene [13], and the $NiCl_3$ monolayer [27]. Yet no Dirac half-metal has been experimentally synthesized [28]. Therefore, the search for spin-polarized Dirac materials with a high possibility of experimental realization is under the spotlight in spin electronics.

The MnF_3 crystal has been fabricated for many years, but no theoretical work reveals its electronic band structure before. In this Letter, we present the experimentally synthesized spin-polarized Dirac material (MnF_3) with promising applications in spintronics. It displays Dirac features in one spin channel, while it possesses a large gap (7.8 eV) in the other spin orientation. This guarantees the generation of a spin-polarized current and spin transport with negligible dissipation. In addition, MnF_3 displays multiple Dirac cones in the band structure instead of a single Dirac cone, and the estimated Fermi velocity of each cone is close to that found in graphene. Strikingly, it exhibits novel rings of Dirac nodes (see Fig. 3) in the Brillouin zone (BZ), which has not been reported in either spin-polarized or conventional Dirac materials. This multiple Dirac ring band dispersion is expected to have more intensive nonlinear electromagnetic

responses [29] than Dirac materials with a single cone, and possess a higher efficiency of carrier transport at the Fermi level via the multiple Dirac channels. Moreover, as the spin-orbital coupling (SOC) is very low in MnF_3, it can easily realize the long distance spin transport for spintronics. Furthermore, we have discovered that the unique electronic properties of MnF_3 are also present in other transition metal fluorides including CoF_3, CrF_3, and FeF_3. The MnF_3-type configuration is expected to be a highly prospective class of candidates for spintronics and enrich the family of novel electronics materials.

All the calculations were performed using density functional theory (DFT) within the Perdew-Burke-Ernzerhof (PBE) parametrization of the generalized gradient approximation (GGA) [30], as implemented in the VASP code [31,32]. Dispersion corrections to the total energy [33] were used to incorporate the long-range van der Waals interaction. A plane-wave basis set with an energy cutoff of 500 eV was employed. The structures were fully optimized until the maximum energy and force were less than 10^{-6} eV and 0.005 eV/Å, respectively. A Monkhorst-Pack k-point mesh of $6 \times 6 \times 2$ was used for geometry optimization. Spin polarization was included through all the calculations and SOC was also considered. The electronic properties of MnF_3 have also been examined by using the DFT + U method [34] and the state-of-the-art Heyd-Scuseria-Ernzerhof (HSE06) functional [35].

The well-studied manganese fluorides [36] include α-MnF_4 (space group, $I41/a$, no. 88) and α-MnF_3 (space group, $C2/c$, No.15). However, little theoretical research has focused on another phase MnF_3 (also named β-MnF_4 in literature) [37,38] despite its experimental synthesis many years ago. The crystal structure of MnF_3 bulk in this work resembles the vanadium (III) fluoride (VF_3) structure type in the hexagonal R-3c space group (no. 167). It contains octahedrally coordinated metal centers with the equal M-F bond lengths of 1.930 Å [Fig. 1(a)]. The optimized lattice constants for MnF_3 are $a = b = 5.20$ Å and $c = 13.46$ Å, respectively. These values are relatively larger than the experimental lattice parameters with $a = b = 4.892$ Å and $c = 13.0$ Å. The unit cell contains 6 Mn and 18 F atoms, respectively. The magnetic moment is found to be 4 μB per formula unit, which is mainly attributed to the transition metal Mn atoms. This can be further verified by plotting the 3D magnetic charge density as shown in Fig. 1(b). Clearly, all magnetic moments are localized around Mn atoms, indicating these atoms are responsible for the magnetic nature of MnF_3.

To determine the magnetic ground state of MnF_3, an energy comparison was made among three different configurations: ferromagnetic (FM), antiferromagnetic (AFM) as well as the nonmagnetic (NM) system. Different magnetic configurations in the $2 \times 2 \times 1$ and $1 \times 1 \times 2$ supercell, and $1 \times 1 \times 1$ unit cell are presented in Figs. S1–S3 of the Supplemental Material [39]. We found the optimized FM state is most energetically stable in all magnetic configurations and it has lower energy than that of the AFM and NM states, respectively. In addition,

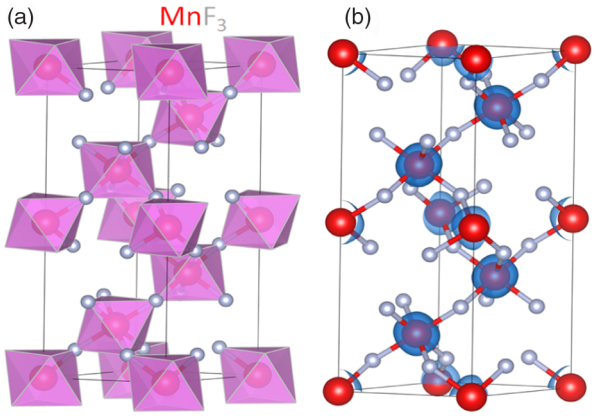

FIG. 1. (a) The crystal structure and (b) 3D magnetic charge density of MnF_3. Key: red, manganese; silver, fluorine; blue, magnetic density.

the remarkable energy difference between FM and NM states indicates very strong magnetism in MnF_3.

Having identified the magnetic ground state of MnF_3, the detailed electronic properties are explained below. The calculated PBE band structures and the Brillouin zone of MnF_3 are illustrated in Figs. 2(a)–2(b), respectively. Without SOC, it can be seen that there are a total of 8 Dirac cones located at or in the vicinity of the Fermi level. Specifically, Dirac cones 1 and 2 are located at the A point and along the A-H line, respectively. As the A-H line is the symmetry line above the Γ-K line, two more cones (3 and 4) are found along the Γ-K line. Although the Γ-M line in reciprocal space is shorter than the Γ-K line, three cones (5, 6, and 7) are found along this line and the last cone (8) is found along the M-L line. If symmetry effects are considered, there would be observed more Dirac cones in the whole BZ. Additionally, all of the Dirac points along the Γ-A and A-H lines are formed by double-degenerate bands as marked by the solid and dotted lines, respectively. In general, the Dirac cones in MnF_3 are protected by the D_{3d} symmetry. A detailed band symmetry analysis is illustrated in Fig. 2(c). It can be clearly seen that bands near the Fermi level belong to two-dimensional irreducible representation E (Table S1). Noticeably, along the wave vector Γ-K, it has a doubly degenerate Dirac cone 4 and a nondegenerate cone 3, which are protected by the group C_{3v}. However, the nondegenerate cone 3 disappears along wave vector A-H due to the symmetry decrease in this line. The large number of Dirac cones and cone degeneracy in MnF_3 are unusual and unique among all reported Dirac materials. As the valence band maximum (VBM) and conduction band minimum (CBM) of the Dirac cones are both contributed to by electrons with the same spin orientation (spin-up), they cannot absolutely touch at the Fermi level because of Pauli repulsion. Therefore a small gap opens for every cone, ranging from 1.4 to 33.8 meV. This gapped Dirac cone feature has been proposed to be a distinctive feature for valley current transport [41]. Considering the electron spin in the band structure, it can be seen that all Dirac cones are contributed to by spin-up orbitals, whereas a 4.1 eV energy gap in the spin-down orientation can be observed [Fig. 2(b)].

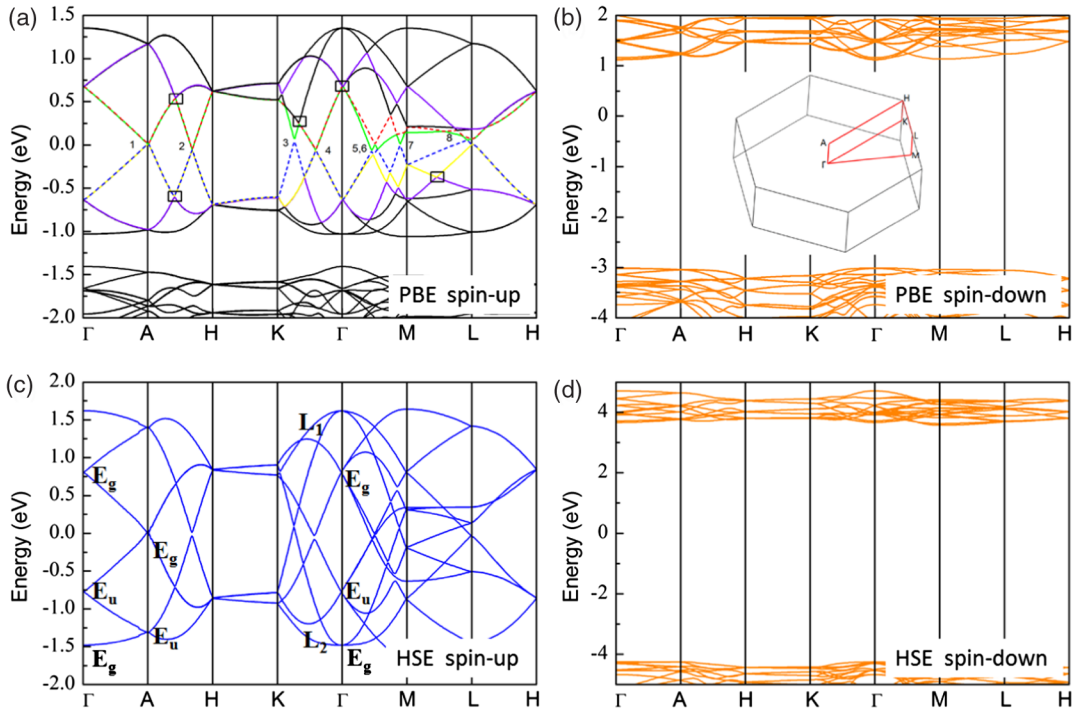

FIG. 2. Band structures of MnF_3 calculated by the (a)–(b) PBE and (c)–(d) HSE06 methods. Dirac cones are distinguished by different numbers and Dirac-like crossings are presented by black squares in (a). Inset of (b) the corresponding Brillouin zone. The irreducible representations of selected bands at the high-symmetric k points are shown in (c) and two specific bands are labeled as L_i ($i = 1, 2$). The Fermi level is set to zero.

When SOC is switched on (Fig. S4 [39]), the linear dispersion of the Dirac cones is hardly affected, only leading to the slight value variation (2.0–15.0 meV) of the opened gaps. In addition, it is also interesting that several Dirac-like crossing points [illustrated in Fig. 2(a) by black squares] are also found above or below the Fermi level. These points are preserved when SOC is considered, which is similar to observations in ZrSiS [42]. As the SOC effect is not significant in its impact on electronic structure, it is expected that MnF_3 possesses a long spin coherence length, and will be an ideal material for spin transport.

It should be noted that the standard DFT is unable to accurately describe the physics of the magnetic transition metal (Mn) with strong correlated d electrons. The DFT + U method is therefore used to examine the band structure of MnF_3. In the spin-up orientation, the DFT + U band structure has negligible difference compared with the PBE bands (Fig. S5a in the Supplemental Material [39]). But for the spin-down channel, the effect of strong correlation of d electrons push the VBM to lower energy and the CBM to higher energy (Fig. S5b [39]), resulting in a larger energy gap of 5.5 eV.

In addition to the DFT + U approach, the highly reliable HSE06 hybrid functional was also employed to yield more accurate band dispersion for MnF_3. As shown in Fig. 2(c), the HSE band curves in the spin-up direction are similar with that of the PBE results, only leading to a slight gap opening of some cones (up to 53.5 meV). It also causes the extension zof bands in energy. For example, the energy difference of band L_1 and L_2 at the Γ point is 3.2 eV by the HSE06 method [Fig. 2(c)] while it is only 2.4 eV according to the PBE result [Fig. 2(a)]. As for the spin-down channel, the HSE06 calculation produces a larger energy gap (7.8 eV) compared with that of the PBE method. To the best of our knowledge, such a substantial energy difference between spin-up and spin-down states has not been reported before and it also demonstrates the spin-down electrons behave like a large gap semiconductor in MnF_3, while in the spin-up orientation electrons it acts as a Dirac material with massless Dirac fermions. Therefore, MnF_3 is expected to be an ideal platform to generate large spin polarization near the Fermi level and greatly increase charge-carrier mobility. The Fermi velocity V_f was calculated through the expression $V_f = \partial E/\hbar\partial k$. The estimated V_f for cones 1–8 ranges from 1.79×10^5 to 3.96×10^5 m/s, which are close to that of graphene. It is also believed the transport efficiency of the polarized electrons in MnF_3 should be higher than the nonpolarized electrons in graphene or other Dirac materials because the electron scattering would be significantly reduced in the single spin channel, leading to a negligible energy loss when electrons are flowing. This is an important aspect that the spin-polarized Dirac cones possess more intriguing properties than the conventional one (e.g., graphene).

The 2D band structure is only capable of characterizing electronic properties along some specific reciprocal space directions. To shed more light on the Dirac feature of the materials in the whole BZ, it is necessary to plot 3D band dispersion. In general, multiple Dirac cone materials display two different behaviors in BZ. The first behavior is

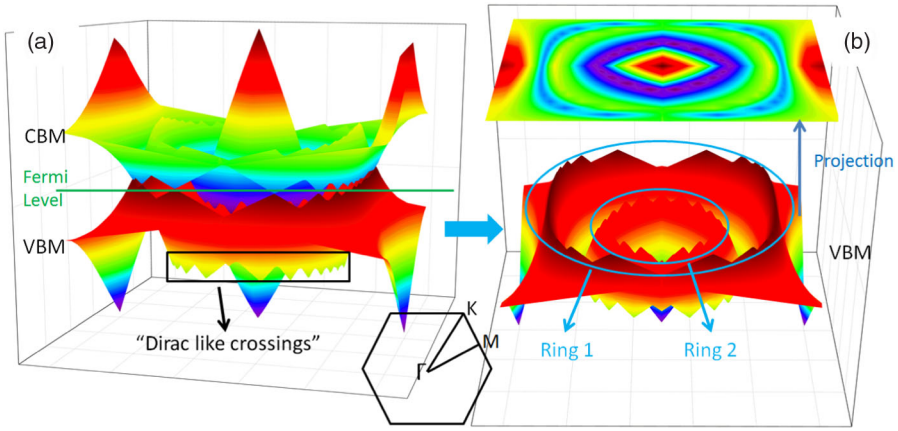

FIG. 3. (a) 3D band plot of MnF_3 in the M-K-Γ plane. (b) The 3D band view of VBM and its corresponding projection.

discontinuous Dirac cones; i.e., the number of cones is countable and they are isolated in the BZ, e.g., the predicted $P6/mmm$ boron sheet [43]. The second case is the continuous Dirac cones, which means a high density of Dirac cones exists and they form a ring of Dirac nodes [44] or a Dirac loop as reported before. As a material with multiple cones, MnF_3 is found to be different from both the above. From the 3D band plots in Fig. 3(a) and 3(b), we can clearly see the MnF_3 displays two rings of Dirac nodes in the M-K-Γ plane of the BZ. Interestingly, if symmetry effect is considered in this bulk material, it is expected to possess additional Dirac ring in the A-H-L plane. Such multiple Dirac ring material is very rare and it differs from the known Dirac materials such as graphene. If we compare the 3D plot with 2D band dispersion in Fig. 2(a), we can find the Dirac cone pair 3 and 7 are responsible for ring 1, and cone 3 and 5 are the origins of ring 2. Furthermore, a ring of Dirac-like crossings [as mentioned in Fig. 2(a)] can also be found below the Fermi level [black square in Fig. 3(a)], which indicates the high carrier mobility of the MnF_3 is not just confined to the Fermi level, but also occurs above or below the Fermi level within the energy range of 0.75 eV. Such a unique multiple Dirac ring feature in MnF_3 is expected to bring about more fascinating electronic properties and applications than other Dirac structures with the single cone or ring.

To gain more insight into the electronic properties of MnF_3 in the vicinity of Fermi level, the spin-resolved total density of states (TDOS) and projected density of states (PDOS) are presented in Fig. 4(a) and 4(b), respectively. From TDOS [Fig. 4(a)], it can be seen that the orbitals near the Fermi level are solely contributed by spin-up electron states. Additionally, the spin-down states are mainly distributed below −4.2 eV and above 3.6 eV, resulting in a large band gap of 7.8 eV. As we can see from Fig. 4(b), the state of Dirac cones at the Fermi level is dominated by the $3d$ spin-up orbital of Mn and is marginally contributed by the $2p$ orbital of F. Notice that sp-electron materials with a single Dirac cone have been extensively studied, but such Dirac material with multiple cones or rings dominated by d electron orbitals has not been seen [45]. The orbital-resolved band structures are also calculated to identify the origin of orbital contributions of different Dirac cones as illustrated in Figs. S6–S8. In general, the cones of MnF_3 are dominated by the hybridization of d_{yz} and d_{xz} electronic states from Mn atoms. In the view of linear combination of atomic orbitals, we also take the Dirac cone 1 as an example and adopt the tight-binding (TB) method to reproduce the electronic bands in the vicinity of the Fermi level and in an attempt to gain more insight into the existence of Dirac cones (see details in the Supplemental Material [39]).

To further test the robustness of Dirac band dispersions in this structure, a pressure up to 6×10^9 Pa were added in MnF_3 (Fig. S10 [39]). We find all Dirac cones were barely affected under such a high pressure, only inducing a moderate change of cone slopes. As the $3d$-orbital plays an important role in forming the Dirac cones in this material, we further investigated the electronics properties

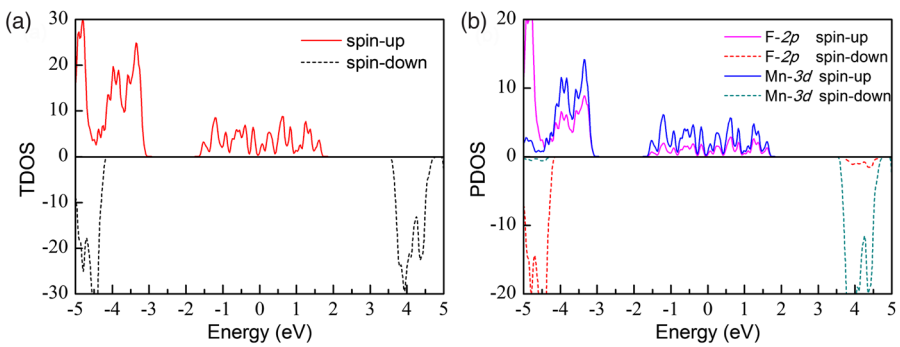

FIG. 4. (a) TDOS and (b) PDOS of MnF_3 by HSE06 calculation. The Fermi level is set to 0.

of some other 3d-transition metal fluorides CoF_3, CrF_3, and FeF_3 as shown in Fig. S11–S13. Large magnetic moments of 3, 3, 5 μB per formula unit can be found in these three structures, respectively. Interestingly, the spin-polarized multiple-Dirac cones are all seen, but they are shifted upwards in energy with respect to the Fermi level.

In conclusion, we report the first example of an experimentally realized material which exhibits spin-polarized multiple Dirac cones or rings in the electronic structure. MnF_3 bridges a gap between Dirac materials and spintronics and it exhibits many unique properties including multiple Dirac rings, large spin polarization, and high carrier mobility. Furthermore, the properties in MnF_3 are intrinsic and do not require any external conditions in experiments such as electric field, pressure, doping, or element substitution. The reported MnF_3 structure meets the requirement of high-efficiency spintronics, and the speed of spin-polarized electrons and holes in MnF_3 should be much faster than previously reported spintronics materials such as spin gapless semiconductor $PbPdO_2$ [22], Mn_2CoAl [23], and diluted magnetic semiconductors. This work is expected to enrich the diversity of spin-polarized Dirac materials and boost the development of spintronics.

The authors thank the grants of high-performance computer time from computing facility at Queensland University of Technology and Australian National Facility. A. D. greatly appreciates the Australian Research Council QEII Fellowship and financial support of the Australian Research Council under Discovery Project (DP130102420).

Y. J. and F. M. contributed equally to this work.

*Corresponding author.
aijun.du@qut.edu.au

[1] C. Chappert, A. Fert, and F. N. Van Dau, Nat. Mater. **6**, 813 (2007).
[2] S. Wolf, D. Awschalom, R. Buhrman, J. Daughton, S. Von Molnar, M. Roukes, A. Y. Chtchelkanova, and D. Treger, Science **294**, 1488 (2001).
[3] I. Žutić, J. Fabian, and S. D. Sarma, Rev. Mod. Phys. **76**, 323 (2004).
[4] D. D. Awschalom and M. E. Flatté, Nat. Phys. **3**, 153 (2007).
[5] K. Sato and H. Katayama-Yoshida, Semicond. Sci. Technol. **17**, 367 (2002).
[6] S. Crooker, M. Furis, X. Lou, C. Adelmann, D. Smith, C. Palmstrøm, and P. Crowell, Science **309**, 2191 (2005).
[7] X. Jiang, R. Wang, R. M. Shelby, R. M. Macfarlane, S. R. Bank, J. S. Harris, and S. S. P. Parkin, Phys. Rev. Lett. **94**, 056601 (2005).
[8] R. Jansen, Nat. Mater. **11**, 400 (2012).
[9] W. Han, R. K. Kawakami, M. Gmitra, and J. Fabian, Nat. Nanotechnol. **9**, 794 (2014).
[10] X. Li, X. Wu, and J. Yang, J. Am. Chem. Soc. **136**, 11065 (2014).
[11] X. Li, X. Wu, and J. Yang, J. Am. Chem. Soc. **136**, 5664 (2014).
[12] X.-L. Wang, S. X. Dou, and C. Zhang, NPG Asia Mater. **2**, 31 (2010).
[13] Y. Li, D. West, H. Huang, J. Li, S. B. Zhang, and W. Duan, Phys. Rev. B **92**, 201403 (2015).
[14] Y. Ma, Y. Dai, X. Li, Q. Sun, and B. Huang, Carbon **73**, 382 (2014).
[15] Y. Li, Z. Zhou, P. Shen, and Z. Chen, ACS Nano **3**, 1952 (2009).
[16] J. Guan, W. Chen, Y. Li, G. Yu, Z. Shi, X. Huang, C. Sun, and Z. Chen, Adv. Funct. Mater. **23**, 1507 (2013).
[17] C. Felser, G. H. Fecher, and B. Balke, *Angew. Chem. Int. Ed.* 46, 668 (2007).
[18] X. Li and J. Yang, Natl. Sci. Rev. **3**, 365 (2016).
[19] X.-L. Wang, Natl. Sci. Rev. **4**, 252 (2017).
[20] A. Du, S. Sanvito, and S. C. Smith, Phys. Rev. Lett. **108**, 197207 (2012).
[21] F. Wu, C. Huang, H. Wu, C. Lee, K. Deng, E. Kan, and P. Jena, Nano Lett. **15**, 8277 (2015).
[22] X. L. Wang, Phys. Rev. Lett. **100**, 156404 (2008).
[23] S. Ouardi, G. H. Fecher, C. Felser, and J. Kübler, Phys. Rev. Lett. **110**, 100401 (2013).
[24] H. Ishizuka and Y. Motome, Phys. Rev. Lett. **109**, 237207 (2012).
[25] X. Zhang, A. Wang, and M. Zhao, Carbon **84**, 1 (2015).
[26] T. Cai, X. Li, F. Wang, S. Ju, J. Feng, and C.-D. Gong, Nano Lett. **15**, 6434 (2015).
[27] J. He, X. Li, P. Lyu, and P. Nachtigall, Nanoscale **9**, 2246 (2017).
[28] Z. F. Wang, Z. Liu, and F. Liu, Phys. Rev. Lett. **110**, 196801 (2013).
[29] C. H. Lee, X. Zhang, and B. Guan, Sci. Rep. **5**, 18008 (2015).
[30] J. P. Perdew, K. Burke, and M. Ernzerhof, Phys. Rev. Lett. **77**, 3865 (1996).
[31] G. Kresse and J. Furthmüller, Phys. Rev. B **54**, 11169 (1996).
[32] G. Kresse and J. Furthmuller, Comput. Mater. Sci. **6**, 15 (1996).
[33] S. Grimme, J. Comput. Chem. **27**, 1787 (2006).
[34] V. I. Anisimov, J. Zaanen, and O. K. Andersen, Phys. Rev. B **44**, 943 (1991).
[35] J. Heyd, G. E. Scuseria, and M. Ernzerhof, J. Chem. Phys. **124**, 219906 (2006).
[36] P. V. Nhat, N. T. Cuong, P. K. Duy, and M. T. Nguyen, Chem. Phys. **400**, 185 (2012).
[37] G. Müller Bernd and M. Serafin, *Zeitschrift für Naturforschung B* 42, 1102 (1987).
[38] Z. Mazej, J. Fluorine Chem. **114**, 75 (2002).
[39] See Supplemental Material at http://link.aps.org/supplemental/10.1103/PhysRevLett.119.016403 for energy comparison of FM, AFM, and NM states and band structures calculated by PBE + SOC, DFT + U, and TB methods as well as orbital-resolved band structures etc., which includes Ref. [40].
[40] J. S. Lim, D. Saldana-Greco, and A. M. Rappe, Phys. Rev. B **94**, 165151 (2016).

[41] Y. D. Lensky, J. C. W. Song, P. Samutpraphoot, and L. S. Levitov, Phys. Rev. Lett. **114**, 256601 (2015).
[42] L. M. Schoop *et al.*, Nat. Commun. **7**, 11696 (2016).
[43] F. Ma, Y. Jiao, G. Gao, Y. Gu, A. Bilic, Z. Chen, and A. Du, Nano Lett. **16**, 3022 (2016).
[44] Y. Jiao, F. Ma, J. Bell, A. Bilic, and A. Du, Angew. Chem. **128**, 10448 (2016).
[45] K. Miyamoto, A. Kimura, K. Kuroda, T. Okuda, K. Shimada, H. Namatame, M. Taniguchi, and M. Donath, Phys. Rev. Lett. **108**, 066808 (2012).